On stochastic study of well capture zones in bounded, randomly heterogeneous media

Zhiming Lu and Dongxiao Zhang

Hydrology, Geochemistry, and Geology Group (EES-6), Los Alamos National Laboratory, Los Alamos, New Mexico, USA

Received 5 August 2002; revised 22 November 2002; accepted 7 February 2003; published 22 April 2003.

[1] Accurately determining well capture zones is of great importance in aquifer cleanup and for the protection of drinking water. Earlier models in delineating capture zones assumed the medium to be homogeneous. Recently, stochastic approaches have been applied to studying capture zones in heterogeneous media. The Monte Carlo method is commonly used to infer the probability distribution of the resulting capture zones from multiple realizations of the aquifer of interest. In this study, we present a moment-equation-based approach to derive the time-dependent mean capture zones and their associated uncertainties. The flow statistics are obtained by solving the first two moments of flow, and the mean capture zones are determined by reversely tracking the nonreactive particles released at a small circle around each pumping well. The uncertainty associated with the mean capture zones is calculated based on the particle displacement covariance X_{ij} for nonstationary flow fields. For comparison purposes, we also conducted Monte Carlo simulations. It has been found that our model results are in excellent agreement with Monte Carlo results. *INDEX TERMS:* 1829 Hydrology: Groundwater hydrology; 1832 Hydrology: Groundwater transport; 1869 Hydrology: Stochastic processes; 3210 Mathematical Geophysics: Modeling; 3230 Mathematical Geophysics: Numerical solutions; *KEYWORDS:* stochastic processes, capture zones, heterogeneity, moment equations, Monte Carlo simulations

Citation: Lu, Z., and D. Zhang, On stochastic study of well capture zones in bounded, randomly heterogeneous media, *Water Resour. Res.*, *39*(4), 1100, doi:10.1029/2002WR001633, 2003.

1. Introduction

[2] Study of well capture zones plays an important role in wellhead protection and designing remediation systems for contaminated aquifers. Many models have been developed in delineating well capture zones. Early models are based on the assumption that the permeability of the porous medium is homogeneous. In this case, analytical solutions may be available. *Bear and Jacobs* [1965] derived an analytical equation for the isochrones of a fully penetrating pumping well in a confined aquifer with a uniform background hydraulic gradient. *Javandel and Tsang* [1987] provided capture-zone type curves for several well placement configurations. *Grubb* [1993] gave analytical solutions for steady state well capture zones in both confined and unconfined aquifers. *Lerner* [1992] investigated the effect of recharge on the well catchments and derived analytical expressions for isochrones in recharged aquifer systems. Other analytical models for capture zones are available for a double well system (pumping-pumping and pumping-injection) [*Zhan*, 1998], two arbitrarily located wells [*Shan*, 1999], horizontal wells [*Zhan*, 1999], and nonsteady state flow conditions [*Yang et al.*, 1995].

[3] *Bhatt* [1993] investigated the influence of the main aquifer properties, such as effective porosity and saturated thickness, on the transverse and longitudinal extent of a capture zone in a confined aquifer. Some other factors that influence the capture zone geometry have been studied including aquifer anisotropy [*Schafer*, 1996; *Bair and Lahm*, 1996; *Zlotnik*, 1997] and partial penetration of pumping wells [*Bair and Lahm*, 1996; *Zlotnik*, 1997].

[4] All above mentioned models in general do not account for the uncertainty of medium properties. In the recent years, several studies have considered the variability of medium properties and the Monte Carlo method has been used in delineating the well capture zone. *Varljen and Shafer* [1991] were the first to apply the stochastic approach to delineating the capture zone. They conducted conditional Monte Carlo simulations to determine the most probable (average) time-related capture zone and its associated uncertainty by averaging the path line endpoints (path lines emanating from the well) at incremental radial directions. *Bair et al.* [1991], assuming that the hydraulic conductivity is a random constant, conducted Monte Carlo simulations to determine percentile confidence regions for given times using convex hulls of the endpoints of reversely-tracked flowpaths emanating from a well. *Cole and Silliman* [1997] performed Monte Carlo simulations of capture zones in heterogeneous unconfined aquifers and used "percentile capture contours" as a measure of the capture zone uncertainty.

[5] *Franzetti and Guadagnini* [1996] and *Guadagnini and Franzetti* [1999] studied the influence of transmissivity heterogeneity on the location of the well catchment using unconditional Monte Carlo simulations. The capture zone probability distribution was inferred from the ensemble of Monte Carlo simulation results. Analogous to the deterministic expression of *Bear and Jacobs* [1965] for capture

zones, they provided an empirical expression that accounts for the transmissivity heterogeneity. *Riva et al.* [1999] investigated the effect of transmissivity variability on the spatial location of time-related capture zones for a conservative tracer in the steady state radial flow field, using a Monte Carlo approach.

[6] *van Leeuwen et al.* [1998] extended this approach by considering capture zones at different times for a fully confined aquifer and a leaky-confined aquifer. A capture zone probability distribution (capd) for a given time is inferred from multiple realizations of capture zones obtained from Monte Carlo simulations. The median isochrone is considered as the preferred statistical measure of the capd's location and the zone of uncertainty for the time is defined as the region within which a particle released has a nonzero probability to reach the well. They also investigated the effect of the transmissivity variance and the correlation scale on well capture zones.

[7] There are several problems with this probability-based approach in delineating well capture zones. The computation effort in this approach can be very large. For each Monte Carlo realization, a particle is released at all grid nodes, requiring numerical computation of a particle trajectory starting from each node until the particle either is captured by the well or reaches the boundary of the flow domain. This algorithm could be even more cumbersome for a system with multiple wells. The limitations of Monte Carlo simulations has been discussed in the literature [e.g., *Tartakovsky et al.*, 1999; *Guadagnini and Neuman*, 1999; *Zhang*, 2002]: the lack of convergence criteria and the requirement of high computational efforts, among others. The computational demand is even large if there are uncertainties in boundary and initial conditions.

[8] *Kunstmann and Kinzelbach* [2000] computed the capture zones using the first-order second moment method on the basis of a Eulerian framework. They derived moment equations for flow and transport equations, and the mean capture zone was defined as the concentration isoline of $c = 0.5$ and the confidence intervals are determined by plus or minus a few standard deviations of concentration. One problem with this algorithm is that it works only for a single well, because in the case of multiple wells it is difficult to distinguish the contributions of different wells to the concentration field. In such a situation, the concentration isoline of $c = 0.5$ may not be appropriate to define the mean capture zones. It is seen from their examples for the cases with a single well that the mean capture zones and the associated confidence intervals are not in good agreement with Monte Carlo simulation results for the unconditional case, even though the variance of the log transmissivity is as low as 0.16.

[9] Recently, *Stauffer et al.* [2002] briefly reported an investigation on the uncertainty quantification of the well capture zones and well catchments in heterogeneous media using a first-order approximation. Specifically, the capture zone of a well for a given time is determined by backward movement of many particles starting near the well, and the uncertainty bandwidth of capture zones is approximated using longitudinal and transversal particle displacement covariances along and normal to the mean particle trajectory. One of limitations in their work is that the nonstationary velocity covariances was approximated by locally scaling the stationary velocity covariance derived by *Rubin* [1990] for uniform mean flows.

[10] Using a Lagrangian approach, *Lu and Zhang* [2003] developed a general stochastic model for transport of conservative solutes in variably saturated nonstationary flow in randomly heterogeneous porous media. The mean flow in the model can be multidirectional and the velocity field can be nonstationary (with location-dependent statistics), which may be caused by statistical nonhomogeneity of medium properties, complex boundary configurations, or pumping or injection. The particle's mean position is determined using the mean Lagrangian velocity. Particle spreading (displacement covariances) is expressed in terms of the state transition matrix that satisfies a time-varying dynamic equation whose coefficient matrix is the derivative of the mean Lagrangian velocity field. In the special cases of stationary velocity fields, their model reduces to the well-known model of *Dagan* [1984, 1989]. For nonstationary but unidirectional flow fields, their model reduces to that of *Butera and Tanda* [1999] and *Sun and Zhang* [2000]. Based on their model, in this study, we present a moment-based stochastic approach to delineate the well capture zones for a system with an arbitrary number of wells (either pumping or injection). Although our approach for flow is Eulerian similar to that of *Kunstmann and Kinzelbach* [2000], our transport approach is cast in a Lagrangian framework. Our model differs from that of *Stauffer et al.* [2002] in that the uncertainty of capture zones in our model is computed from the particle displacement covariances for nonstationary flow fields. A certain number of particles are released around each pumping well. The first-order mean capture zones around each pumping well are delineated using the first-order mean flow velocity. The confidence intervals of capture zones can be derived from the particle displacement covariance for nonstationary flows [*Lu and Zhang*, 2003]. The validity of our model is confirmed by comparisons with Monte Carlo simulations for several cases with one or two pumping wells. An excellent agreement is found between our model results and those from Monte Carlo simulations.

2. Mathematical Formulation

[11] We consider water flow in saturated media satisfying the following continuity equation and Darcy's law:

$$-\nabla \cdot \mathbf{q}(\mathbf{x}, t) + \sum_{j=1}^{n_w} Q_j \delta(\mathbf{x} - \mathbf{x}_j) = S_s \frac{\partial h(\mathbf{x}, t)}{\partial t}, \tag{1}$$

$$\mathbf{q}(\mathbf{x}, t) = -K(\mathbf{x}) \nabla h(\mathbf{x}, t), \tag{2}$$

subject to initial and boundary conditions

$$h(\mathbf{x}, 0) = h_0(\mathbf{x}), \qquad \mathbf{x} \in \Omega \tag{3}$$

$$h(\mathbf{x}, t) = h_1(\mathbf{x}, t), \qquad \mathbf{x} \in \Gamma_D \tag{4}$$

$$\mathbf{q}(\mathbf{x}, t) \cdot \mathbf{n}(\mathbf{x}) = Q(\mathbf{x}, t), \qquad \mathbf{x} \in \Gamma_N. \tag{5}$$

Here the Darcian flux $\mathbf{q}(\mathbf{x})$ $[LT^{-1}]$, the saturated hydraulic conductivity $K(\mathbf{x})[LT^{-1}]$ and the hydraulic head gradient $\nabla h(\mathbf{x}, t)$ are representative of a bulk support volume ω centered about a point $\mathbf{x} = (x_1, \cdots, x_d)^T$, such that ω is small compared to the flow domain Ω but is sufficiently large for

(1)–(5) to be locally valid [*Neuman and Orr*, 1993; *Tartakovsky et al.*, 1999]. The volume ω does not need to be an REV in the traditional sense [*Bear*, 1972]. The only requirement is that all quantities in (1)–(5) are measurable at the support scale ω inside the domain Ω and on its boundary Γ, which is the union of Dirichlet boundary Γ_D and Neumann boundary Γ_N. Here n_w is the number of pumping (or injection) wells, Q_j is the pumping (or injection) rate of the j^{th} well located at $\mathbf{x}_j = (x_{j1}, \ , x_{jd})^T$, δ is the Dirac delta function, S_s is the specific storage, $h_0(\mathbf{x})$ is the initial pressure head in the domain Ω, $h_1(\mathbf{x}, t)$ is the prescribed head on Dirichlet boundary segments Γ_D, $Q(\mathbf{x}, t)$ is the prescribed flux across Neumann boundary segments Γ_N, and $\mathbf{n}(\mathbf{x}) = (n_1, \cdots, n_d)^T$ is an outward unit vector normal to the boundary. The velocity field $\mathbf{V}(\mathbf{x}, t)$ is related to the specific discharge $\mathbf{q}(\mathbf{x}, t)$ and porosity ϕ: $\mathbf{V}(\mathbf{x}, t) = \mathbf{q}(\mathbf{x}, t)/\phi$.

2.1. First-Order Moment Equations

[12] First-order moment equations for flow in unsaturated/saturated porous media have been developed by *Zhang and Lu* [2002], and they can be easily reduced to equations for saturated flow. However, for completeness, in this section we briefly outline the procedure. For simplicity, in this study, we assume that porosity ϕ, specific storage S_s, and all boundary and initial conditions are deterministic. For random boundary and initial conditions, the readers are referred to *Zhang and Lu* [2002] for details. Again, we assume that the hydraulic conductivity $K(\mathbf{x})$ follows a log normal distribution, and work with the log-transformed variable $Y(\mathbf{x}) = \ln(K(\mathbf{x})) = \langle Y(\mathbf{x})\rangle + Y'(\mathbf{x})$. The mean log saturated hydraulic conductivity $\langle Y(\mathbf{x})\rangle$ represents a relatively smooth unbiased estimate of the unknown random function $Y(\mathbf{x})$. It may be estimated using standard geostatistical methods, such as kriging, which produce unbiased estimates that honor measurements and provide uncertainty measures for these estimates. Here we assume that the log saturated hydraulic conductivity field may be conditioned at some measurement points, which means that the field may be statistically inhomogeneous.

[13] Because the variability of $h(\mathbf{x}, t)$ depends on the input variability, i.e., the variability of $Y(\mathbf{x})$, one may express $h(\mathbf{x}, t)$ as an infinite series as $h(\mathbf{x}, t) = h^{(0)} + h^{(1)} + h^{(2)} + \cdots$. In this series, the order of each term is with respect to σ_Y, the standard deviation of $Y(\mathbf{x})$. After combining (1) and (2), substituting expansions of $h(\mathbf{x}, t)$ and $Y(\mathbf{x})$, and collecting terms at separate order, and after some mathematical manipulations, one can obtain the following equations governing the first two moments of head [*Zhang*, 2002],

$$\frac{\partial^2 h^{(0)}(\mathbf{x},t)}{\partial x_i^2}+\frac{\partial\langle Y(\mathbf{x})\rangle}{\partial x_i}\frac{\partial h^{(0)}(\mathbf{x},t)}{\partial x_i}+\sum_{j=1}^{n_w}\frac{Q_j}{K_G(\mathbf{x})}\delta(\mathbf{x}-\mathbf{x}_j) = \frac{S_s}{K_G(\mathbf{x})}\frac{\partial h^{(0)}(\mathbf{x},t)}{\partial t}, \tag{6}$$

$$\begin{aligned} h^{(0)}(\mathbf{x},0) &= \langle h_0(\mathbf{x})\rangle, \qquad \mathbf{x}\in\Omega \\ h^{(0)}(\mathbf{x},t) &= \langle h_1(\mathbf{x},t)\rangle, \qquad \mathbf{x}\in\Gamma_D,\ t>0 \\ n_i(\mathbf{x})\frac{\partial h^{(0)}(\mathbf{x},t)}{\partial x_i} &= -\langle Q(\mathbf{x},t)\rangle/K_G(\mathbf{x}), \qquad \mathbf{x}\in\Gamma_N, t>0, \end{aligned} \tag{7}$$

and

$$\begin{aligned} \frac{\partial^2 C_h(\mathbf{x},t;\boldsymbol{\chi},\tau)}{\partial x_i^2}+\frac{\partial\langle Y(\mathbf{x})\rangle}{\partial x_i}\frac{\partial C_h(\mathbf{x},t;\boldsymbol{\chi},\tau)}{\partial x_i} &= \frac{S_s}{K_G(\mathbf{x})}\frac{\partial C_h(\mathbf{x},t;\boldsymbol{\chi},\tau)}{\partial t} \\ &- \frac{\partial h^{(0)}(\mathbf{x},t)}{\partial x_i}\frac{\partial C_{Yh}(\mathbf{x};\boldsymbol{\chi},\tau)}{\partial x_i} - C_{Yh}(\mathbf{x};\boldsymbol{\chi},\tau) \\ &\cdot\left[\frac{\partial^2 h^{(0)}(\mathbf{x},t)}{\partial x_i^2}+\frac{\partial\langle Y(\mathbf{x})\rangle}{\partial x_i}\frac{\partial h^{(0)}(\mathbf{x},t)}{\partial x_i}\right], \end{aligned} \tag{8}$$

$$\begin{aligned} C_h(\mathbf{x},0;\boldsymbol{\chi},\tau) &= 0, \quad \mathbf{x}\in\Omega \\ C_h(\mathbf{x},t;\boldsymbol{\chi},\tau) &= 0, \quad \mathbf{x}\in\Gamma_D,\ t>0 \\ n_i(\mathbf{x})\left[\frac{\partial C_h(\mathbf{x},t;\boldsymbol{\chi},\tau)}{\partial x_i}+C_{Yh}(\mathbf{x};\boldsymbol{\chi},\tau)\frac{\partial h^{(0)}(\mathbf{x},t)}{\partial x_i}\right] &= 0, \\ \mathbf{x}\in\Gamma_N, t>0, \end{aligned} \tag{9}$$

where $C_{Yh}(\boldsymbol{\chi}; \mathbf{x}, t)$ can be obtained by solving the following equations [*Zhang*, 2002]

$$\begin{aligned} \frac{\partial^2 C_{Yh}(\boldsymbol{\chi};\mathbf{x},t)}{\partial x_i^2}+\frac{\partial\langle Y(\mathbf{x})\rangle}{\partial x_i}\frac{\partial C_{Yh}(\boldsymbol{\chi};\mathbf{x},t)}{\partial x_i} &= \frac{S_s}{K_G(\mathbf{x})}\frac{\partial C_{Yh}(\boldsymbol{\chi};\mathbf{x},t)}{\partial t} \\ &- \frac{\partial h^{(0)}(\mathbf{x},t)}{\partial x_i}\frac{\partial C_Y(\boldsymbol{\chi};\mathbf{x})}{\partial x_i} - C_Y(\boldsymbol{\chi};\mathbf{x}) \\ &\cdot\left[\frac{\partial^2 h^{(0)}(\mathbf{x},t)}{\partial x_i^2}+\frac{\partial\langle Y(\mathbf{x})\rangle}{\partial x_i}\frac{\partial h^{(0)}(\mathbf{x},t)}{\partial x_i}\right], \end{aligned} \tag{10}$$

$$\begin{aligned} C_{Yh}(\boldsymbol{\chi},\mathbf{x},0) &= 0, \quad \mathbf{x}\in\Omega \\ C_{Yh}(\boldsymbol{\chi};\mathbf{x},t) &= 0, \quad \mathbf{x}\in\Gamma_D, t>0 \\ n_i(\mathbf{x})\left[\frac{\partial C_{Yh}(\boldsymbol{\chi};\mathbf{x},t)}{\partial x_i}+C_Y(\boldsymbol{\chi};\mathbf{x})\frac{\partial h^{(0)}(\mathbf{x},t)}{\partial x_i}\right] &= 0, \\ \mathbf{x}\in\Gamma_N,\ t>0. \end{aligned} \tag{11}$$

The first two moments of the flux are

$$\mathbf{q}^{(0)}(\mathbf{x},t) = -K_G(\mathbf{x})\nabla_{\mathbf{x}}h^{(0)}(\mathbf{x},t), \tag{12}$$

$$\begin{aligned} C_{\mathbf{q}}(\mathbf{x},t;\boldsymbol{\chi},\tau) &= K_G(\mathbf{x})K_G(\boldsymbol{\chi})[C_Y(\mathbf{x};\boldsymbol{\chi})\nabla_{\mathbf{x}}h^{(0)}(\mathbf{x},t)\nabla_{\boldsymbol{\chi}}^T h^{(0)}(\boldsymbol{\chi},\tau) \\ &+ \nabla_{\mathbf{x}}h^{(0)}(\mathbf{x},t)\nabla_{\boldsymbol{\chi}}^T C_{Yh}(\mathbf{x};\boldsymbol{\chi},\tau) + \nabla_{\mathbf{x}}C_{Yh}(\boldsymbol{\chi};\mathbf{x},t) \\ &\cdot\nabla_{\boldsymbol{\chi}}^T h^{(0)}(\boldsymbol{\chi},\tau) + \nabla_{\mathbf{x}}\nabla_{\boldsymbol{\chi}}^T C_h(\mathbf{x},t;\boldsymbol{\chi},\tau)]. \end{aligned} \tag{13}$$

It can be shown that $\langle h^{(0)}(\mathbf{x}, t)\rangle \equiv h^{(0)}(\mathbf{x}, t)$ and $\langle h^{(1)}(\mathbf{x}, t)\rangle \equiv 0$, thus the mean head solution up to zeroth-order or first-order is $h^{(0)}(\mathbf{x}, t)$. The mean flux is $\mathbf{q}^{(0)}(\mathbf{x}, t)$ to zeroth order or first-order. The second-order correction terms $\langle h^{(2)}(\mathbf{x}, t)\rangle$ and $\langle \mathbf{q}^{(2)}(\mathbf{x}, t)\rangle$ can be given similarly [*Zhang*, 2002]. The velocity covariance can be derived through $C_{\mathbf{v}}(\mathbf{x}, t; \boldsymbol{\chi}, \tau) = C_{\mathbf{q}}(\mathbf{x}, t; \boldsymbol{\chi}, \tau)/[\phi(\mathbf{x})\phi(\boldsymbol{\chi})]$ upon assuming deterministic porosity ϕ. Here both $C_{\mathbf{q}}$ and $C_{\mathbf{v}}$ are tensors (usually asymmetric).

2.2. Mean Trajectory and Displacement Covariance

[14] For a given flow field, the trajectory of a particle located at $\mathbf{a}$ at $t = t_0$ is described by the following kinetic equation:

$$\frac{d\mathbf{X}(t;\mathbf{a},t_0)}{dt} = \mathbf{V}[\mathbf{X}(t;\mathbf{a},t_0)], \tag{14}$$

subject to the initial condition $\mathbf{X}(t_0;\mathbf{a},t_0)=\mathbf{a}$, where $\mathbf{X}(t;\mathbf{a},t_0)$ stands for the particle position at time t and $\mathbf{V}[\mathbf{X}(t;\mathbf{a},t_0)]$ denotes the (Lagrangian) velocity of the particle. Up to first-order, the mean trajectory $\langle\mathbf{X}_t\rangle$ and its associated perturbation $\mathbf{X}'_t = (X'_{t,1}, \cdots, X'_{t,d})^T$ for nonstationary flow field have been given [see *Lu and Zhang*, 2003]:

$$\frac{d\langle\mathbf{X}_t\rangle}{dt} = \langle\mathbf{V}(\langle\mathbf{X}_t\rangle)\rangle, \tag{15}$$

subject to the initial condition $\langle\mathbf{X}_t\rangle = \mathbf{a}$, and

$$\frac{dX'_{t,i}}{dt} = V'_i(\langle\mathbf{X}_t\rangle) + B_{ij}(t)X'_{t,j}, \quad i = 1,\cdots,d \tag{16}$$

with the initial condition $\mathbf{X}'_t = \mathbf{X}'_0 = (X'_{0,1}, , X'_{0,d})^T$ at $t = t_0$, the particle displacement at the initial time t_0. Summation for repeated indices in (16) is implied. B_{ij} in (16) is the derivative of the mean velocity in the i^{th} direction with respect to particle's position $X_{t,j}$, evaluated at the particle's mean position at time t:

$$B_{ij}(t) = \left.\frac{\partial\langle V_i(\mathbf{X}_t)\rangle}{\partial X_{t,j}}\right|_{\mathbf{X}_t=\langle\mathbf{X}_t\rangle}. \tag{17}$$

The displacement covariance then can be obtained from (16) as [*Lu and Zhang*, 2003]

$$\begin{aligned}\langle\mathbf{X}'_t\mathbf{X}'^T_t\rangle &= \Phi(t,t_0)\langle\mathbf{X}'_0\mathbf{X}'^T_0\rangle\Phi^T(t,t_0)\\ &+ \int_{t_0}^{t}\Phi(t,t_0)\langle\mathbf{X}'_0\mathbf{V}'^T(\langle\mathbf{X}_{\tau'}\rangle)\rangle\Phi^T(t,\tau')d\tau'\\ &+ \int_{t_0}^{t}\Phi(t,\tau)\langle\mathbf{V}'(\langle\mathbf{X}_\tau\rangle)\mathbf{X}'^T_0\rangle\Phi^T(t,t_0)d\tau\\ &+ \int_{t_0}^{t}\int_{t_0}^{t}\Phi(t,\tau)\left\langle\mathbf{V}'(\langle\mathbf{X}_\tau\rangle)\mathbf{V}'^T(\langle\mathbf{X}_{\tau'}\rangle)\right\rangle\Phi^T(t,\tau')d\tau'd\tau.\end{aligned} \tag{18}$$

Here $\mathbf{V}' = (V'_1, \cdots, V'_d)^T$ is the velocity perturbation, and the $d \times d$ matrix $\Phi(t, t_0)$ is called the state transition matrix (or fundamental matrix), which satisfies the homogeneous equation

$$\frac{d\Phi(t,t_0)}{dt} = \mathbf{B}(t)\Phi(t,t_0), \tag{19}$$

subject to the initial condition $\Phi(t_0, t_0) = E$, where E is the identity matrix. If the displacement perturbation at the initial state $\mathbf{X}'_0 \equiv 0$, for instance at the time of a known release ($t_0 \equiv 0$), (18) simplifies to

$$\left\langle\mathbf{X}'_t\mathbf{X}'^T_t\right\rangle = \int_{t_0}^{t}\int_{t_0}^{t}\Phi(t,\tau)\left\langle\mathbf{V}'(\langle\mathbf{X}_\tau\rangle)\mathbf{V}'^T(\langle\mathbf{X}_{\tau'}\rangle)\right\rangle\Phi^T(t,\tau')d\tau'd\tau \tag{20}$$

or in its component form

$$\begin{aligned}X_{ij}(t) &= \left\langle X'_{t,i}X'_{t,j}\right\rangle\\ &= \int_{t_0}^{t}\int_{t_0}^{t}\Phi_{ik}(t,\tau)\Phi_{jl}(t,\tau')\left\langle V'_k(\langle\mathbf{X}_\tau\rangle)V'_l(\langle\mathbf{X}_{\tau'}\rangle)\right\rangle d\tau d\tau'.\end{aligned} \tag{21}$$

If the spatial variation of the mean velocity is ignored, (21) reduces to following equation, similar to the well-known expression of *Dagan* [1984, 1989]:

$$X_{ij}(t) = \left\langle X'_{t,i}X'_{t,j}\right\rangle = \int_{t_0}^{t}\int_{t_0}^{t}\left\langle V'_k(\langle\mathbf{X}_\tau\rangle)V'_l(\langle\mathbf{X}_{\tau'}\rangle)\right\rangle d\tau d\tau'. \tag{22}$$

In our first example of section 4, we will demonstrate the difference in estimation of capture zone uncertainty due to using (21) and (22). For nonstationary but unidirectional flow fields, (21) reduces to that of *Butera and Tanda* [1999] and *Sun and Zhang* [2000].

[15] Note that except for the singular points in the flow field, (21) is also valid for the reverse particle tracking, simply by negating the velocity field. In the terminology of *Zhang and Neuman* [1995], the particle displacement covariance may be called "particle origin covariance."

3. Numerical Implementation

[16] Unless for some special cases, the moment equations (6)–(11) cannot, in general, be solved analytically. Numerical implementation of these equations has been discussed in detail by *Zhang and Winter* [1998]. Upon solving (6)–(11), the first-order mean Eulerian velocity field and velocity covariance can be calculated from (12)–(13).

[17] For a particle released at location X_0 at time $t = 0$, the first-order mean Lagrangian velocity field and its covariance can be derived based on the first-order mean Eulerian velocity field and velocity covariances. The mean trajectory up to first-order may be obtained by solving (15). The derivatives of the first-order mean Lagrangian velocity field with respect to the mean trajectory (along the particle path), $B_{ij}(t)$, can be calculated by numerically taking derivative of the mean Lagrangian velocity field.

[18] It is worthy to note that, in general, there is no simple analytical expression for $\Phi(t, \tau)$ (unless $\mathbf{B}$ is time-invariant or diagonal, which yields the respective result of $\Phi(t, \tau) = \exp[\mathbf{B}(t - \tau)]$ or $\Phi(t, \tau) = \exp[\int_\tau^t \mathbf{B}(t')dt']$), the moments X_{ij} have to be evaluated numerically, which requires evaluation of the state transition matrix $\Phi(t, \tau)$ for certain values of t and τ. *Lu and Zhang* [2003] proposed an algorithm to compute $\Phi(t, \tau)$. When the flow field is highly nonuniform, for example, in the presence of pumping or injection wells, it is difficult to calculate $\Phi(t, \tau)$ with desired accuracy, mainly due to errors introduced in numerically computing matrix $\mathbf{B}$.

[19] In some special cases, however, the first-order approximation of the $\mathbf{B}$ matrix can be derived analytically, instead of calculating it numerically by taking derivatives of the first-order mean velocity field. Here we propose two simple possible approaches to compute matrix $\mathbf{B}$. If the porous medium is statistically homogeneous and the flow domain is rectangular, $0 \le x_1 \le L_1$ and $0 \le x_2 \le L_2$, the first-order steady state mean head field (and thus the

velocity field and the **B** matrix) may be obtained analytically, as shown in Appendix A for the case with prescribed hydraulic heads on the left and right boundaries, and impermeable boundaries on two lateral sides. In this case, from (A9) one has

$$B_{11}(x_1,x_2)=\frac{1}{L_1\phi}\sum_{m=1}^{\infty}\alpha_m\sin(\alpha_m x_1)\sum_{i=1}^{n_w}Q_i\sin(\alpha_m x_{i1})\times\frac{\cosh[\alpha_m(L_2-(x_2+x_{i2}))]+\cosh[\alpha_m(L_2-|x_2-x_{i2}|)]}{\sinh(\alpha_m L_2)}, \tag{23}$$

$$B_{12}(x_1,x_2)=\frac{1}{L_1\phi}\sum_{m=1}^{\infty}\alpha_m\cos(\alpha_m x_1)\sum_{i=1}^{n_w}Q_i\sin(\alpha_m x_{i1})\times\frac{\sinh[\alpha_m(L_2-(x_2+x_{i2}))]+sign(x_2-x_{i2})\sinh[\alpha_m(L_2-|x_2-x_{i2}|)]}{\sinh(\alpha_m L_2)}, \tag{24}$$

where α_m and β_n are defined in Appendix A. Similarly, from (A10) we have

$$B_{21}(x_1,x_2)=-\frac{1}{L_2\phi}\sum_{n=1}^{\infty}\beta_n\sin(\beta_n x_2)\sum_{i=1}^{n_w}Q_i\cos(\beta_n x_{i2})\times\frac{sign(x_1-x_{i1})\sinh[\beta_n(L_1-|x_1-x_{i1}|)]-\sinh[\beta_n(L_1-(x_1-x_{i1}))]}{\sinh(\beta_n L_1)}, \tag{25}$$

$$B_{22}(x_1,x_2)=\frac{1}{L_2\phi}\sum_{n=1}^{\infty}\beta_n\sin(\beta_n x_2)\sum_{i=1}^{n_w}Q_i\cos(\beta_n x_{i2})\times\frac{\cosh[\beta_n(L_1-|x_1-x_{i1}|)]+\cosh[\beta_n(L_1-(x_1+x_{i1}))]}{\sinh(\beta_n L_1)}. \tag{26}$$

From (A8) it is easy to see that $B_{12} = B_{21}$. Based on the continuity equation, except for the well locations, one has the relation $B_{11} = -B_{22}$. Therefore, to determine the **B** matrix, one needs only to know either B_{11} and B_{12}, or B_{21} and B_{22}. However, numerical calculation of (23)–(26) may be tricky. If x_2 is close to or equal to any one of x_{i2}, $i = 1, \cdots, n_w$, (23) and (24) are hard to converge or do not converge at all. In this case, one has to employ (25) and (26). Similarly, If x_1 is close to or equal to any one of x_{i1}, $i = 1, \cdots, n_w$, one has to employ (23) and (24).

[20] In the cases that the flow domain is not rectangular but the porous medium is still statistically homogeneous, a first-order analytical expression for matrix **B** may be derived using the potential theory, as shown in Appendix B. Taking partial derivatives of v_1 and v_2 in (B3) and (B4) with respect to x_1 and x_2, we have

$$B_{11}(x_1,x_2)=\frac{\partial v_1}{\partial x_1}=-\sum_{k=1}^{n_w}\frac{Q_k}{2\phi\pi r_k^2}\left[1-\frac{2(x_1-x_{k1})^2}{r_k^2}\right], \tag{27}$$

$$B_{12}(x_1,x_2)=\frac{\partial v_1}{\partial x_2}=\sum_{k=1}^{n_w}\frac{Q_k}{2\phi\pi r_k^2}\frac{2(x_1-x_{k1})(x_2-x_{k2})}{r_k^2}=B_{21}(x_1,x_2), \tag{28}$$

$$B_{22}(x_1,x_2)=\frac{\partial v_2}{\partial x_2}=-\sum_{k=1}^{n_w}\frac{Q_k}{2\phi\pi r_k^2}\left[1-\frac{2(x_2-x_{k2})^2}{r_k^2}\right]=-B_{11}(x_1,x_2), \tag{29}$$

where $r_k^2=(x_1-x_{k1})^2+(x_2-x_{k2})^2$. It should be pointed out that, though (B2) is derived for homogeneous media with infinite extent and a mean uniform regional flow, B_{ij} is independent of the mean uniform regional flow and depends only on the pumping (or injection) rate and the distance between the particle and well locations. When the particle is far away from the well, B_{ij} approaches zero, as is expected for the mean uniform regional flow.

4. Construction of Capture Zones and Their Uncertainties

[21] In this study, the time-dependent well capture zones are determined by reverse particle tracking. For a flow field with pumping wells, streamlines (or path lines) converge to pumping wells and thus the flow field has singularities at the well locations. In the process of reverse particle tracking, if a particle is located at a pumping well, it is impossible to track it reversely and to tell where the particle came from. As a result, a small $r > 0$ is selected and particles are released at a circle of radius r around the well. Particles are arranged around each pumping well in such a way that more particles are on the down gradient direction of the mean uniform background flow. For example, if the uniform background flow is from the right to the left, more particles will be placed at the left side of pumping wells. The reason for this is that, for the mean flow field, because the stagnation points are located in the downstream side of the wells, those particles released around wells may quickly move to the upstream direction (in reverse tracking), which causes difficulty in constructing late-time capture zones (only one particle possibly remaining at the stagnation point of each pumping well at later time), unless they are placed very close to the points immediately left of wells. These particles close to the immediately left of each pumping well will take much longer time to exit the system, which allows us to construct late-time capture zones more easily.

[22] The mean trajectories $\langle X_i(t)\rangle$ and displacement covariance $X_{ij}(t)$ are then computed based on (15) and (21) for all particles released around all pumping wells. For a pumping well located at (x_{w1}, x_{w2}), the mean position $\langle X_i\rangle$ and displacement covariance X_{ij} at any time for any released particle are then converted to the local polar coordinates centered at the well location. The first-order mean distance $\langle R\rangle$ from the well, its variance σ_R^2, and the first-order mean angle $\langle\theta\rangle$ from x_1 axis (the right direction) are computed from the mean trajectories $\langle X_i\rangle$ and the displacement covariance X_{ij} according to the following formulae (see Appendix C):

$$\langle R\rangle=\sqrt{(\langle X_1\rangle-x_{w1})^2+(\langle X_2\rangle-x_{w2})^2}, \tag{30}$$

$$\sigma_R^2=\Big[(\langle X_1\rangle-x_{w1})^2X_{11}+(\langle X_2\rangle-x_{w2})^2X_{22}+2(\langle X_1\rangle-x_{w1})\rangle\cdot(\langle X_2\rangle-x_{w2})X_{12}\Big]/\langle R\rangle^2, \tag{31}$$

$$\tan(\langle\theta\rangle) = \frac{\langle X_2\rangle - x_{w2}}{\langle X_1\rangle - x_{w1}}. \quad (32)$$

[23] For any elapsed time, the curve that connects the endpoints of the mean trajectories ($\langle R\rangle$, $\langle\theta\rangle$) of all particles released around the well is considered the position of the mean capture zone for this well at the given time. The capture zone intervals at the 95% confidence level are constructed using the $\langle R\rangle$ plus and minus 1.96 σ_R along the direction $\langle\theta\rangle$. Strictly speaking, if the distribution of distance R in the local polar coordinates at any time is not normal, then plus or minus a few standard deviations from $\langle R\rangle$ may not be appropriate to represent confidence intervals. For a log normal distribution, we may compute $\langle R\rangle$ and σ_R from $\langle X_i\rangle$ and X_{ij} using (30)–(32), and then obtain $\langle\ln(R)\rangle$ and σ_{lnR} according to

$$\sigma^2_{lnR} = \ln\left(1 + \frac{\sigma^2_R}{\langle R\rangle^2}\right), \quad (33)$$

$$\langle\ln(R)\rangle = \ln(\langle R\rangle) - \frac{1}{2}\,\sigma^2_{lnR}. \quad (34)$$

We may then calculate its q^{th} quantile $r_q = \exp[\langle\ln(R)\rangle + \sigma_{lnR}\, a_q]$, where $a_q = F^{-1}(q)$, $q \in [0, 1]$, and F^{-1} is the inverse cumulative density function of the standard normal distribution. By q^{th} quantile r_q, we mean that fraction q of points below the given value r_q. For example, the 0.975 quantile, $r_{0.975}$, is the value at which 97.5% of data fall below and 2.5% fall above this value. For the given 95% confidence level, the region defined by $r_{0.025}$ and $r_{0.975}$ may be used as the confidence interval.

5. Illustrative Examples

[24] To illustrate the proposed approach in determining the time-dependent well capture zones and examine the validity of our approach, we consider a two-dimensional rectangular domain in a saturated heterogeneous porous medium. The flow domain has a length $L_1 = 20$ [L] (where L is any consistent length unit) and a width $L_2 = 12$ [L], uniformly discretized into 50×30 square elements of a size 0.16 [L^2]. The statistics of the log hydraulic conductivity are given as $\langle Y\rangle = 0.0$ (i.e., the geometric mean saturated hydraulic conductivity $K_G = 1.0$ [L/T], where T is any consistent time unit), $\sigma^2_Y = 0.5$, $\lambda_Y = 2.0$ [L], which equals the length of five elements. The no-flow conditions are prescribed at two lateral boundaries. The hydraulic head is prescribed at the left and right boundaries as 10.0 [L] and 10.5 [L], respectively, which produces a background flow from the right to the left. In the first example, denoted as case 1, a pumping well is located at (4.8 [L], 6.0 [L]) with a pumping rate of $Q_w = 0.16$ [L^3/T].

[25] For the purpose of comparison, we conducted Monte Carlo simulations. We generated 5,000 two-dimensional 51×31 (the hydraulic conductivity values are assigned at nodes) unconditional Gaussian realizations with a zero mean, a unit variance, and a correlation length $\lambda = 2.0$ [L], using a sequential Gaussian random field generator sgsim from GSLIB [*Deutsch and Journel*, 1998]. These realizations are then scaled to the specified mean and variance of the log hydraulic conductivity.

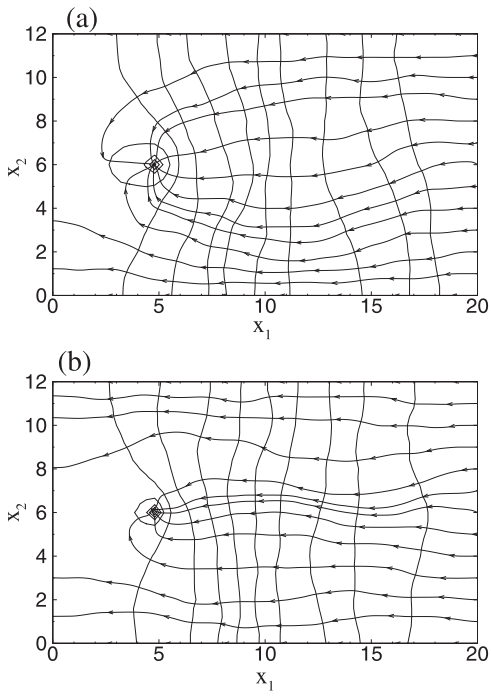

Figure 1. Two steady state capture zones from two Monte Carlo realizations.

[26] The saturated steady state flow equation is solved for each generated realization of log hydraulic conductivity, using the Finite element Heat- and Mass transfer code (FEHM) developed by *Zyvoloski et al.* [1997]. Figure 1 depicts two realizations of flow fields for case 1, indicating that there is a large variation in capture zones among individual realizations. For each realization, once the flow field is solved, the velocity is negated and 42 nonreactive particles are placed on a circle of $r = 0.4$ [L] around the well in the way as described in section 4. More specifically, in the local polar coordinates originated in each pumping well location, 6 particles are uniformly located on the arc of $0° \sim 100°$ on the cycle, where 0° points to the upstream direction, 3 particles on the arc of $110° \sim 130°$, 8 particles on $135° \sim 170°$, and 5 particles on $172° \sim 180°$. The particles on the other half of the cycle (the arc of $180° \sim 360°$) are symmetrically placed. We recorded each particle's position at some given times until it leaves the domain. The mean position of any particle and its spreading (displacement covariance X_{ij}) at any given time are then calculated using the particle's position at that time from all realizations. Because the particle released from a given point may leave the flow domain earlier in some realizations than in others, we calculated the mean particle position and its spreading only up to the maximum time at which the particle remains within the flow domain for all simulations. The scattering of particles for any given time in all Monte Carlo simulations is compared against the mean capture zone and its confidence intervals at the same time resulted from the moment-based approach, as a measure of validity of our moment-based approach.

[27] Figure 2 illustrates histograms of R at $t = 10$ T at radial directions $\theta = 0°$ and $\theta = 180°$ with a tolerance

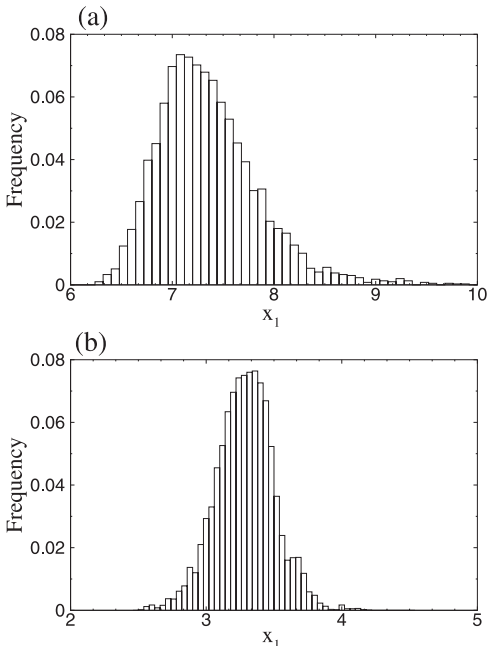

Figure 2. Histograms of R, the radial distance of the particle from the well, at (a) the upstream and (b) downstream directions at $t = 10T$ for case 1.

of $\Delta\theta = 1.0°$. It is shown from Figure 2 that the distribution of particles in the upstream direction of the mean uniform background flow is more or less log normal (Figure 2a), while close to normal in the downstream direction (Figure 2b). This implies that, in constructing the 95% confidence intervals of capture zones in our moment approach, we may need to use $r_{0.025}$ and $r_{0.975}$, instead of plus or minus $1.96\sigma_R$.

[28] In our examples, we use the sample mean velocity field and sample velocity covariances calculated from Monte Carlo simulations as the input Eulerian mean velocity field and velocity covariances to the first-order stochastic transport model. We do so to ensure that the stochastic transport model and the Monte Carlo transport simulations have the same underlying flow field and are thus compatible. Therefore the causes for any difference between the two sets of results would be the truncation errors in neglecting higher-order terms in the first-order stochastic transport model, the numerical errors associated with approximating the first-order expressions and with particle tracking in the Monte Carlo simulations, and the statistical sampling errors occurred in the Monte Carlo simulations.

[29] The mean flow field for case 1 is illustrated Figure 3, where the dashed lines are equipotential lines and the solid lines with arrows are streamlines. Particles are then released in the mean flow field at the same locations as in Monte Carlo simulations. The particles' mean positions and their displacement covariance at any time then can be calculated using (15) and (21). The mean capture zones (Figure 3, heavy lines with times marked) and confidence intervals are then constructed with the procedure shown in section 4.

[30] In practice, if a particle is captured by a well, its trajectory is not our major concern. However, to illustrate the validity of our model, we compared several particles' mean trajectories $\langle X_i \rangle$ and displacement covariance X_{ij} obtained using Monte Carlo simulations and the moment-

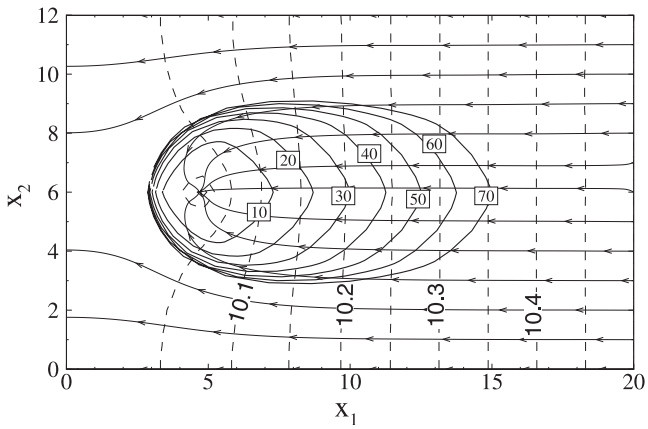

Figure 3. The mean flow and mean capture zones at different times for case 1.

based approach, as shown in Figures 4–5. Figure 4 shows the mean trajectories of two particles released at $r = 0.4$ [L], $\theta = 60°$ and $\theta = 100°$ in the local polar coordinates centered at the well location, where MC and ME stand for the results from Monte Carlo simulations and the moment-equation-based approach, respectively. Relatively short curves for MC results are due to the fact that once a particle reaches the boundary at a certain time in one Monte Carlo realization, we are not able to compute this particle's mean position thereafter.

[31] Figure 5 depicts comparison of the displacement covariance X_{11} and X_{22} derived from Monte Carlo simulations and our moment-based approach (using the potential theory in calculating the **B** matrix) along the above mentioned two trajectories. Also compared in Figure 5 are

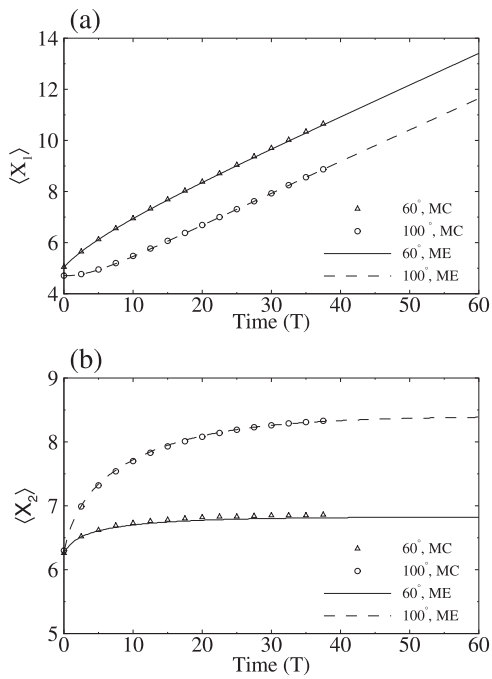

Figure 4. Comparison of Monte Carlo simulations and the moment approach on the mean positions of two particles released at the angle of 60° and 100°, for case 1: (a) $\langle X_1 \rangle$, and (b) $\langle X_2 \rangle$.

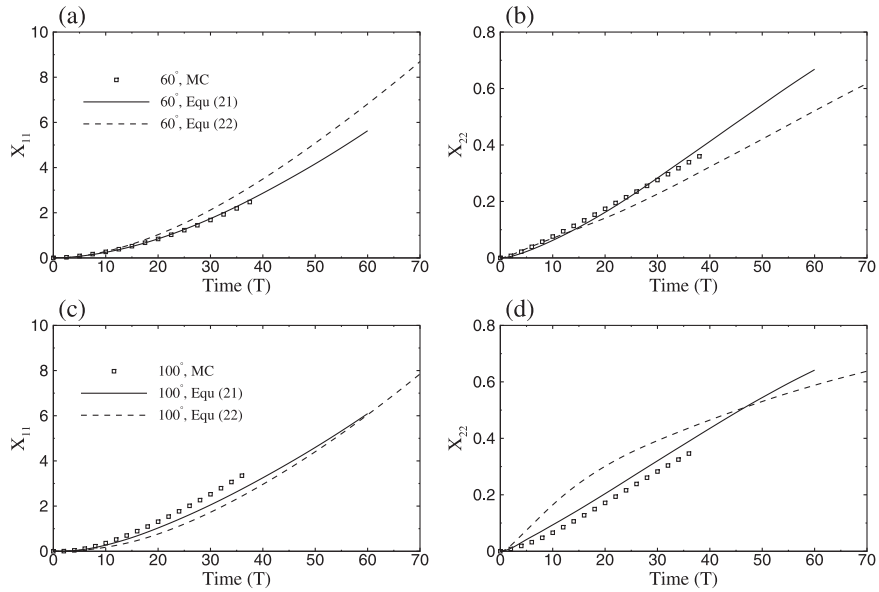

Figure 5. Comparison of Monte Carlo simulations with the moment approach using (21) and the moment approach using (22) on the displacement covariance of two particles released at the angle of 60° and 100° for case 1: (a) X_{11}, θ = 60°, (b) X_{22}, θ = 60°, (c) X_{11}, θ = 100°, and (d) X_{22}, θ = 100°.

X_{11} and X_{22} derived by ignoring spatial the variation of the mean velocity field, i.e., using (22). Figure 5 shows that in general X_{11} and X_{22} computed using Monte Carlo simulations and moment-based approaches are close, especially when the effect of the nonuniform mean velocity field is included, i.e., using (21). Figure 5 also indicates that a relatively large error may be introduced if the spatial variation of the mean velocity is ignored, i.e., using (22). When the particle's mean position is far away from the well, although the effect of the uniform mean background flow will be dominant (i.e., **B** = 0 and Φ = *E*), (21) should still be used in calculating displacement covariance X_{ij}, because the moments $X_{ij}(t)$ account for accumulative effects from the time when the particle was released till the current time *t*.

[32] Figures 6a and 6b compare scattering plots of Monte Carlo results (dots) at $t = 10\ T$ and $t = 20\ T$ against the confidence intervals (at the 95% confidence level) computed by adding or subtracting $1.96\sigma_R$ to the mean capture zones at these elapsed times, where σ_R is the standard deviation of the radial distance *R* from the well, calculated using (31). Figures 6a and 6b indicate that at the 95% confidence level, the confidence intervals can capture the

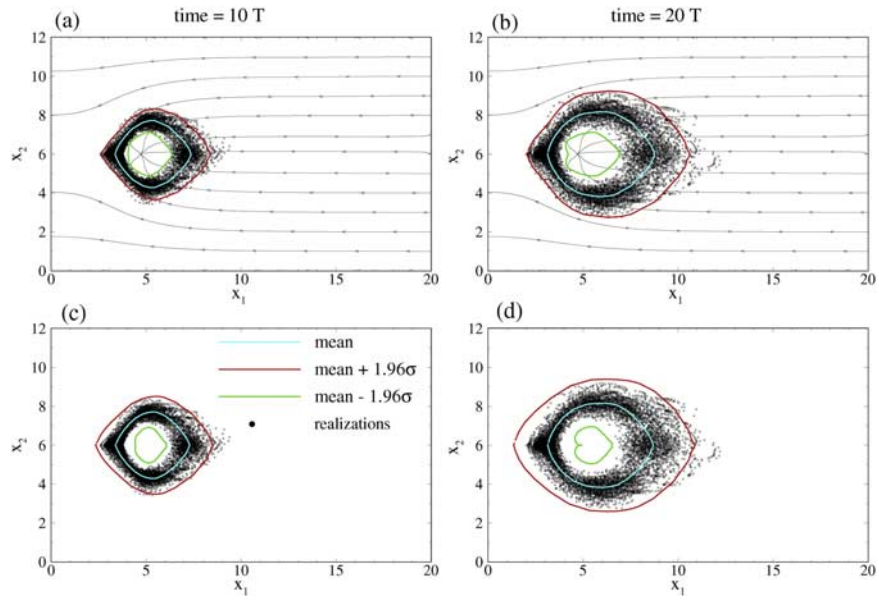

Figure 6. Comparison of Monte Carlo simulations (dots) against the moment approach using (21) or (22) on the mean capture zones and the 95% confidence intervals (assuming *R* to be normal) at two times, for case 1, (a) using (21) at time $t = 10\ T$, (b) using (21) at time $t = 20\ T$, (c) using (22) at time $t = 10\ T$, and (d) using (22) at time $t = 20\ T$.

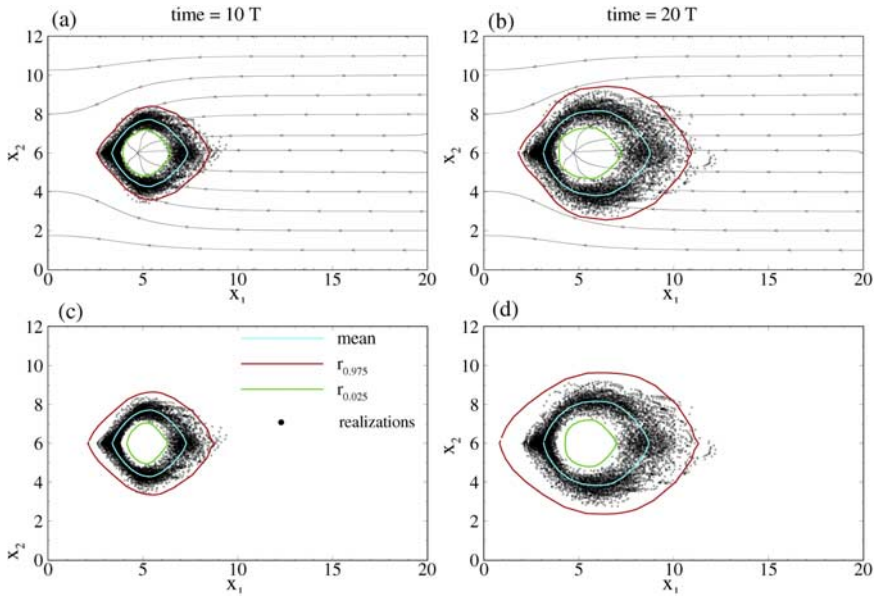

Figure 7. Comparison of Monte Carlo simulations (dots) against the moment approach using (21) or (22) on the mean capture zones and the 95% confidence intervals (assuming R to be lognormal) at two times, for case 1, (a) using (21) at time $t = 10\ T$, (b) using (21) at time $t = 20\ T$, (c) using (22) at time $t = 10\ T$, and (d) using (22) at time $t = 20\ T$.

possible capture zones extremely well, especially at early time. However, if the spatial variation of the mean velocity field is ignored (i.e., $\mathbf{B} \equiv 0$, $\Phi \equiv E$) and (22) is used, the calculated 95% confidence intervals do not match the Monte Carlo results very well, as shown Figures 6c and 6d for the same elapsed times $t = 10\ T$ and $t = 20\ T$.

[33] Similar to Figure 6, Figure 7 shows comparisons between the particle spreading from Monte Carlo simulations and confidence intervals derived with/without considering the effect of spatial variation of the mean velocity field, assuming that the distribution of particles along the radial direction from the well is lognormal. From Figures 5 and 6 it seems that the upper bound of the confidence interval can be well represented by $\langle R \rangle + 1.96\sigma_R$, while the lower bound may be matched better by $r_{0.025}$.

[34] In the second example (case 2), two pumping wells are placed at (4.8 [L], 4.8 [L]) and (10.0 [L], 6.4 [L]) with pumping rates of 0.08 [L^3/T] and 0.16 [L^3/T], respectively. The properties of the porous medium and boundary configurations are the same as those in case 1. Figure 8 depicts the mean capture zones of two wells at different times, while Figure 9 shows the mean capture zones at $t = 5\ T$ and predicted uncertainties represented by the mean capture zones plus and minus 1.96 σ_R. Figure 9 also compares the uncertainty computed from the moment approach with the Monte Carlo simulations. It is seen from Figure 9 that mean capture zones and their associated uncertainties derived from our moment approach are in excellent agreement with Monte Carlo results. Figure 10 illustrate the similar data but at time $t = 10\ T$.

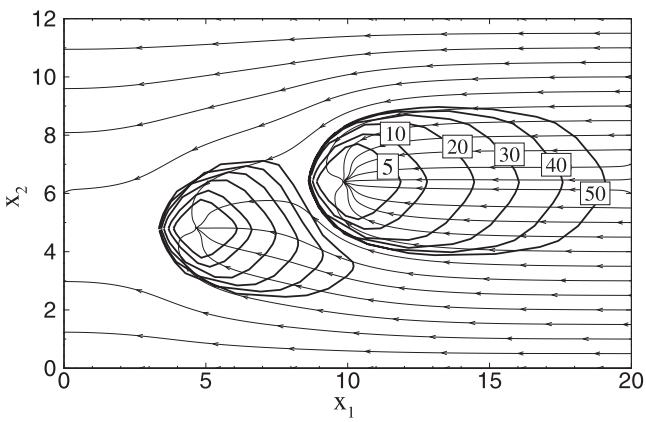

Figure 8. The mean flow and mean capture zones at different times for case 2.

6. Summary and Conclusions

[35] This paper leads to the following major conclusions.

[36] 1. It is possible to apply the stochastic moment approach to the construction of well capture zones and their uncertainties for multiple wells (pumping or injection) with

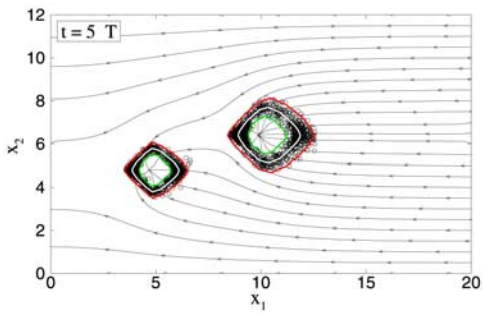

Figure 9. Comparison of Monte Carlo simulations (dots) against the moment approach using (21) on the mean capture zones and the 95% confidence intervals (assuming R to be normal) at the time $t = 5\ T$, for case 2.

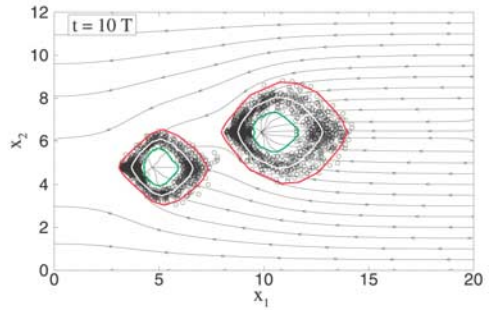

Figure 10. Comparison of Monte Carlo simulations (dots) against the moment approach using (21) on the mean capture zones and the 95% confidence intervals (assuming R to be normal) at the time $t = 10\ T$, for case 2.

a uniform background flow in bounded randomly heterogeneous porous media. The flow statistics are obtained by solving the first two moments of flow, and the mean capture zones are determined by reversely tracking the nonreactive particles released at a small circle around each pumping well. The uncertainty associated with the mean capture zones is determined by the particle displacement covariance X_{ij} developed for nonstationary flow fields [*Lu and Zhang*, 2003].

[37] 2. The results based on our moment approach are in excellent agreement with Monte Carlo simulation results. However, the moment approach is computationally more efficient. First, as discussed in literature, for the Monte Carlo simulation, a large number of runs are required to obtain a statistically convergent solution. In addition, for each Monte Carlo run, the particles are placed in each node of the numerical grid and then particle tracking is performed for all these particles. In our moment approach, a certain number of particles (much less than the number of nodes in the numerical grid) are placed only around each pumping well.

[38] 3. The well-known expression of Dagan [1984, 1989] for the displacement covariance, which was originally derived under stationary flow conditions, does not work well in the presence of pumping or injection wells. When the mean flow field is highly nonstationary, as in the cases shown in this paper, the expression of *Lu and Zhang* [2003] should be used.

[39] 4. Though the examples we showed here are for two-dimensional saturated flows, this methodology is not restricted to two-dimensional saturated flows and can be applied to three-dimensional saturated/unsaturated flows.

Appendix A

[40] For two-dimensional flow in a saturated statistically homogeneous porous medium with the boundary conditions as described in case 1, the first-order mean equation (6) can be rewritten as

$$\left(\frac{\partial^2 H(x_1,x_2,t)}{\partial x_1^2}+\frac{\partial^2 H(x_1,x_2,t)}{\partial x_2^2}\right)+\sum_{i=1}^{n_w}\frac{Q_i}{T_G}\delta(x_1-x_{1i})\delta(x_2-x_{2i}) = \frac{S}{T_G}\frac{\partial H(x_1,x_2,t)}{\partial t}, \tag{A1}$$

subject to boundary and initial conditions:

$$\begin{aligned} H(0,x_2,t) &= H_1, \quad 0\le x_2\le L_2, t>0 \\ H(L_1,x_2,t) &= H_2, \quad 0\le x_2\le L_2, t>0 \\ \partial H(x_1,x_2,t)/\partial x_2|_{x_2=0} &= 0, \quad 0\le x_1\le L_1, t>0 \\ \partial H(x_1,x_2,t)/\partial x_2|_{x_2=L_2} &= 0, \quad 0\le x_1\le L_1, t>0 \\ H(x_1,x_2,0) &= H_1+(H_2-H_1)x_1/L_1, \end{aligned} \tag{A2}$$

where T_G is the geometric mean of the transmissivity, S is the storitivity, n_w is the number of wells, and Q_i is the pumping (or injection) rate of the i^{th} well located at (x_{i1}, x_{i2}). Note that the pumping (or injection) rate Qi here is the integration of the rate Q_i in (6) along the entire aquifer thickness. Under the given boundary conditions, by using the integral transformation [*Özişik*, 1989]

$$H^*(\alpha_m,\beta_n,t)=\int_0^{L_1}\int_0^{L_2}k(\alpha_m,x_1)k(\beta_n,x_2)\,H(x_1',x_2',t)dx_1'dx_2', \tag{A3}$$

where kernels $k(\alpha_m,x_1)=\sqrt{2/L_1}\sin(\alpha_m x_1), k(\beta_n,x_2)=\sqrt{2/L_2}\cos(\beta_n x_2)$ for $n\neq 0$ and $k(\beta_n,x_2)=\sqrt{1/L_2}$ for $n=0$, $\alpha_m=m\pi/L_1$, $m=1, 2, \cdots$, $\beta_n=n\pi/L_2$, $n=0, 1, \cdots$, (A1) is transformed to

$$\frac{dH^*(\alpha_m,\beta_n,t)}{dt}+\frac{T_G}{S}(\alpha_m^2+\beta_n^2)H^*(\alpha_m,\beta_n,t)=A(\alpha_m,\beta_n,t), \tag{A4}$$

with the initial condition

$$H^*(\alpha_m,\beta_n,0)\begin{cases}\sqrt{\dfrac{2L_2}{L_1}}\dfrac{H_1-(-1)^m H_2}{\alpha_m} & \text{if n}=0\\ 0 & \text{otherwise.}\end{cases} \tag{A5}$$

The term on the right-hand side of (A4) is the transformation of boundary conditions and source/sink terms. The first-order ordinary differential equation (A4) with its initial condition (A5) can be solved easily and its solution can be converted to the solution of (A1)–(A2) through

$$H(x_1,x_2,t)=\sum_{m=1}^{\infty}\sum_{n=0}^{\infty}e^{-\frac{T_G}{S}(\alpha_m^2+\beta_n^2)t}k(\alpha_m,x_1)k(\beta_n,x_2)\cdot H^*(\alpha_m,\beta_n,t). \tag{A6}$$

Thus

$$\begin{aligned} H(x_1,x_2,t) &= H_1+\frac{H_2-H_1}{L_1}x_1+\frac{2}{L_1L_2T_G}\sum_{m=1}^{\infty}\frac{\sin(\alpha_m x_1)}{\alpha_m^2}\cdot\sum_{i=1}^{n_w}Q_i\sin(\alpha_m x_{i1})\left(1-e^{-\frac{T_G}{S}\alpha_m^2 t}\right)\\ &+\frac{4}{L_1L_2T_G}\sum_{m,n=1}^{\infty}\frac{\sin(\alpha_m x_1)\cos(\beta_n x_2)}{\alpha_m^2+\beta_n^2}\cdot\sum_{i=1}^{n_w}Q_i\sin(\alpha_m x_{i1})\cos(\beta_n x_{i2})\left(1-e^{-\frac{T_G}{S}(\alpha_m^2+\beta_n^2)t}\right). \end{aligned} \tag{A7}$$

The steady state solution can be obtained by letting t approach infinity:

$$H(x_1,x_2,\infty) = H_1 + \frac{H_2-H_1}{L_1}x_1 + \frac{2}{L_1L_2T_G}\sum_{m=1}^{\infty}\frac{\sin(\alpha_m x_1)}{\alpha_m^2} \cdot \sum_{i=1}^{n_w} Q_i \sin(\alpha_m x_{i1}) + \frac{4}{L_1L_2T_G}\sum_{m,n=1}^{\infty}\frac{\sin(\alpha_m x_1)\cos(\beta_n x_2)}{\alpha_m^2+\beta_n^2} \cdot \sum_{i=1}^{n_w} Q_i \sin(\alpha_m x_{i1})\cos(\beta_n x_{i2}). \quad \text{(A8)}$$

If we take the second derivatives of H in (A8) with respect to x_1 and x_2, the derived formal series may not converge. To avoid this, summing up the series in (A8) with respect to index n and using some mathematical equalities [*Gradshteyn and Ryzhik*, 1980], one can rewrite (A8) as

$$H(x_1,x_2,\infty) = H_1 + \frac{H_2-H_1}{L_1}x_1 + \frac{1}{L_1T_G} \cdot \sum_{m=1}^{\infty}\frac{\sin(\alpha_m x_1)}{\alpha_m}\sum_{i=1}^{n_w} Q_i \sin(\alpha_m x_{i1}) \times \frac{\cosh[\alpha_m(L_2-(x_2+x_{i2}))]+\cosh[\alpha_m(L_2-|x_2-x_{i2}|)]}{\sinh(\alpha_m L_2)}. \quad \text{(A9)}$$

As taking the second derivative of H in (A9) with respect to x_2 is not easy, we can write an equivalent form of (A9) by summing up series in (A8) with respect to index m first,

$$H(x_1,x_2,\infty) = H_1 + \frac{H_2-H_1}{L_1}x_1 + \frac{1}{2L_1L_2T_G} \cdot \sum_{i=1}^{n_w} Q_i[L_1(x_{i1}+x_1-|x_{i1}-x_1|)-2x_{i1}x_1] + \frac{1}{L_2T_G}\sum_{n=1}^{\infty}\frac{\cos(\beta_n x_2)}{\beta_n}\sum_{i=1}^{n_w} Q_i\cos(\beta_n x_{i2}) \cdot \frac{\cosh[\beta_n(L_1-(x_1+x_{i1}))]-\cosh[\beta_n(L_1-|x_1-x_{i1}|)]}{\sinh(\beta_n L_1)}. \quad \text{(A10)}$$

Equations (A8)–(A10) are three alternative forms of solution of hydraulic head in a homogeneous porous medium with boundary conditions given in (A2). It should be noted that (A8)–(A10) are also first-order (or zeroth-order) solutions for mean hydraulic head in a heterogeneous porous medium, with boundary conditions (A2). Therefore the first-order approximation of **B** matrix can be derived by taking the second derivatives of head H in (A9) or (A10) with respect to x_1 and x_2.

[41] For the boundary conditions other than those shown in (A2), similar transformations as (A3) can be used upon replacing with appropriate kernels [*Özişik*, 1989].

Appendix B

[42] The complex potential for a homogeneous unbounded system with a well in a uniform horizontal regional flow has been given [e.g., *Bear*, 1972; *Strack*, 1989; *Grubb*, 1993] and can be extended, based on superposition, to a system with n_w wells located at (x_{k1}, x_{k2}), $k = 1,2, \cdots, n_w$

$$\Omega = -Q_0 z e^{-i\alpha} + \sum_{k=1}^{n_w}\frac{Q_k}{2\pi}\ln(z-z_k) + C \quad \text{(B1)}$$

Here Q_0 is the discharge of the uniform flow, $z = x_1 + ix_2$, $z_k = x_{k1} + ix_{k2}$, $i = \sqrt{-1}$, α is the angle between the x_1 axis and the uniform flow, Q_k is the discharge rate from the k^{th} well, and C is a constant. The real part of (B1) is called the discharge potential (traditionally denoted as Φ, using Ψ here to avoid confusion with the transition matrix Φ)

$$\Psi(x_1,x_2) = -Q_0[x_1\cos\alpha + x_2\sin\alpha] + \sum_{k=1}^{n_w}\frac{Q_k}{2\pi}\ln(r_k) \quad \text{(B2)}$$

where $r_k = [(x_1 - x_{k1})^2 + (x^2 - x_{k2})^2]^{1/2}$. The velocity component in the i^{th} direction can be derived from the first partial derivative of the discharge potential with respect to x_i:

$$v_1(x_1,x_2) = -\frac{1}{\phi}\frac{\partial\Psi(x_1,x_2)}{\partial x_1} = \frac{Q_0}{\phi}\cos\alpha - \sum_{k=1}^{n_w}\frac{Q_k}{2\phi\pi}\frac{x_1-x_{k1}}{r_k^2} \quad \text{(B3)}$$

$$v_2(x_1,x_2) = -\frac{1}{\phi}\frac{\partial\Psi(x_1,x_2)}{\partial x_2} = \frac{Q_0}{\phi}\sin\alpha - \sum_{k=1}^{n_w}\frac{Q_k}{2\phi\pi}\frac{x_2-x_{k2}}{r_k^2} \quad \text{(B4)}$$

where ϕ is porosity.

[43] The velocities v_1 are v_2 are functions of time t through the particle's position x_1 and x_2. Taking partial derivatives of v_i with respect to x_1 and x_2, one obtains matrix **B**.

Appendix C

[44] For a particle located at $\mathbf{X} = (X_1, X_2)^T$, the distance between $\mathbf{X}$ and the well location $\mathbf{x}_w = (x_{w1}, x_{w2})^T$ is

$$R = \sqrt{(X_1-x_{w1})^2+(X_2-x_{w2})^2}. \quad \text{(C1)}$$

Writing $X_i = \langle X_i\rangle + X_i'$, and expanding (C1) using Taylor expansion up to the first order terms, one has

$$R = \sqrt{(\langle X_1\rangle - x_{w1})^2+(\langle X_2\rangle - x_{w2})^2} \cdot \left(1+\frac{(\langle X_1\rangle - x_{w1})X_1' + (\langle X_2\rangle - x_{w2})X_2'}{(\langle X_1\rangle - x_{w1})^2+(\langle X_2\rangle - x_{w2})^2}\right). \quad \text{(C2)}$$

Taking the ensemble mean yields

$$\langle R\rangle = \sqrt{(\langle X_1\rangle - x_{w1})^2+(\langle X_2\rangle - x_{w2})^2}. \quad \text{(C3)}$$

From (C2) and (C3), the first-order fluctuation of R is

$$R' = \left[(\langle X_1\rangle - x_{w1})X_1' + (\langle X_2\rangle - x_{w2})X_2'\right]/\langle R\rangle \quad \text{(C4)}$$

and thus the variance σ_R^2 can be derived from (C4) as

$$\sigma_R^2 = \left[(\langle X_1\rangle - x_{w1})^2 X_{11} + (\langle X_2\rangle - x_{w2})^2 X_{22} + 2(\langle X_1\rangle - x_{w1}) \cdot (\langle X_2\rangle - x_{w2})X_{12}\right]/\langle R\rangle^2. \quad \text{(C5)}$$

The angle from the x_1-axis to the particle position can be found as

$$\tan(\theta) = \frac{X_2 - x_{w2}}{X_1 - x_{w1}}. \tag{C6}$$

Expanding both sides of (C6) gives

$$\tan(\langle\theta\rangle) + \theta'/\cos^2(\langle\theta\rangle) = \frac{1}{\langle X_1\rangle - x_{w1}} \cdot \left[\langle X_2\rangle - x_{w2} - \frac{\langle X_2\rangle - x_{w2}}{\langle X_1\rangle - x_{w1}} X_1' + X_2'\right] \tag{C7}$$

Taking the ensemble mean yields

$$\tan(\langle\theta\rangle) = \frac{\langle X_2\rangle - x_{w2}}{\langle X_1\rangle - x_{w1}}. \tag{C8}$$

Subtracting (C8) from (C7), one obtains the perturbation of θ

$$\theta' = \frac{\langle X_1\rangle - x_{w1}}{\langle R\rangle^2}\left[X_2' - \frac{\langle X_2\rangle - x_{w2}}{\langle X_1\rangle - x_{w1}} X_1'\right] \tag{C9}$$

and the variance σ_θ^2

$$\sigma_\theta^2 = \frac{(\langle X_1\rangle - x_{w1})^2}{\langle R\rangle^4}\left[X_{22} + \frac{(\langle X_2\rangle - x_{w2})^2}{(\langle X_1\rangle - x_{w1})^2} X_{11} + 2\frac{(\langle X_2\rangle - x_{w2})}{(\langle X_1\rangle - x_{w1})} X_{12}\right]. \tag{C10}$$

References

Bair, E. S., and T. D. Lahm, Variations in capture-zone geometry of a partially penetrating pumping well in an unconfined aquifer, *Ground Water*, *34*(5), 842–852, 1996.

Bair, E. S., C. M. Safreed, and E. A. Stasny, A Monte Carlo-based approach for determining traveltime-related capture zones of wells using convex hulls as confidence regions, *Ground Water*, *29*, 849–855, 1991.

Bear, J., *Dynamics of Fluids in Porous Media*, Dover, Mineola, N. Y., 1972.

Bear, J., and M. Jacobs, On the movement of water bodies injected into aquifers, *J. Hydrol.*, *3*, 37–57, 1965.

Bhatt, K., Uncertainty in wellhead protection area delineation due to uncertainty in aquifer parameter values, *J. Hydrol.*, *149*, 1–8, 1993.

Butera, I., and M. G. Tanda, Solute transport analysis through heterogeneous media in nonuniform in the average flow by a stochastic approach, *Transp. Porous Media*, *36*, 255–291, 1999.

Cole, B. E., and S. E. Silliman, Capture zones for passive wells in heterogeneous unconfined aquifers, *Ground Water*, *35*(1), 92–98, 1997.

Dagan, G., Solute transport in heterogeneous porous formations, *J. Fluid Mech.*, *145*, 151–177, 1984.

Dagan, G., *Flow and Transport in Porous Formations*, Springer-Verlag, New York, 1989.

Deutsch, C. V., and A. G. Journel, *GSLIB: Geostatistical Software Library*, 340 pp., Oxford Univ. Press, New York, 1998.

Franzetti, S., and A. Guadagnini, Probabilistic estimation of well catchments in heterogeneous aquifers, *J. Hydrol.*, *174*, 149–171, 1996.

Gradshteyn, I. S., and I. M. Ryzhik, *Table of Integrals, Series, and Products*, Academic, San Diego, Calif., 1980.

Grubb, S., Analytical model for estimation of steady-state capture zones of pumping wells in confined and unconfined aquifers, *Ground Water*, *31*(1), 27–32, 1993.

Guadagnini, A., and S. Franzetti, Time-related capture zones for contaminants in randomly heterogeneous formations, *Ground Water*, *37*(2), 253–260, 1999.

Guadagnini, A., and S. P. Neuman, Nonlocal and localized analyses of conditional mean steady state flow in bounded, randomly nonuniform domains: 1. Theory and computational approach, *Water Resour. Res.*, *35*(10), 2999–3018, 1999.

Javandel, I., and C.-F. Tsang, Capture-zone type curves: A tool for aquifer cleanup, *Ground Water*, *24*(5), 616–625, 1987.

Kunstmann, H., and W. Kinzelbach, Computation of stochastic wellhead protection zones by combining the first-order second-moment method and Kolmogorov backward equation analysis, *J. Hydrol.*, *237*, 127–146, 2000.

Lerner, D. N., Well catchments and time-of-travel zones in aquifers with recharge, *Water Resour. Res.*, *28*(10), 2621–2628, 1992.

Lu, Z., and D. Zhang, Solute spreading in nonstationary flows in bounded, heterogeneous unsaturated-saturated media, *Water Resour. Res.*, *39*(3), 1049, doi:10.1029/2001WR000908, 2003.

Neuman, S. P., and S. Orr, Prediction of steady state flow in nonuniform geologic media by conditional moments: Exact nonlocal formalism, effective conductivities, and weak approximation, *Water Resour. Res.*, *29*(2), 341–364, 1993.

Özişik, M. N., *Boundary Value Problems of Heat Conduction*, Dover, Mineola, N. Y., 1989.

Riva, M., A. Guadagnini, and F. Ballio, Time-related capture zones for radial flow in two-dimensional randomly heterogeneous media, *Stochastic Environ. Res. Risk Assess.*, *13*(3), 217–230, 1999.

Rubin, Y., Stochastic modeling of macrodispersion in heterogeneous porous media, *Water Resour. Res.*, *26*(1), 133–141, 1990.

Schafer, D. C., Determining 3D capture zones in homogeneous, anisotropic aquifers, *Ground Water*, *34*(4), 1996.

Shan, C., An analytical solution for the capture zone of two arbitrarily located wells, *J. Hydrol.*, *222*, 123–128, 1999.

Stauffer, F., S. Attinger, S. Zimmermann, and W. Kinzelbach, Uncertainty estimation of well head protection zones: A Lagrangian approximation, paper presented at the International Groundwater Symposium, Int. Assoc. for Hyrdraul. Res., Berkeley, Calif., 2002.

Strack, O. D. L., Groundwater Mechanics, Prentice-Hall, Old Tappan, N. J., 1989.

Sun, A. Y., and D. Zhang, Prediction of solute spreading during vertical infiltration in unsaturated, bounded heterogeneous porous media, *Water Resour. Res.*, *36*(3), 715–723, 2000.

Tartakovsky, D. M., S. P. Neuman, and Z. Lu, Conditional stochastic averaging of steady state unsaturated flow by means of Kirchhoff transformation, *Water Resour. Res.*, *35*(3), 731–745, 1999.

van Leeuwen, M., C. B. M. te Stroet, A. P. Butle, and J. A. Tompkins, Stochastic determination of well capture zones, *Water Resour. Res.*, *34*(9), 2215–2223, 1998.

Varljen, M. D., and J. M. Shafer, Assessment of uncertainty in time-related capture zones using conditional simulation of hydraulic conductivity, *Ground Water*, *29*, 737–748, 1991.

Yang, Y. J., R. D. Spencer, and T. M. Gates, Analytical solutions for determination of non-steady-state and steady-state capture zones, *Ground Water Monit. Rem.*, *15*, 101–106, 1995.

Zhan, H., Analytical and numerical modeling of a double well capture zone, *Math. Geol.*, *31*(2), 175–193, 1998.

Zhan, H., Analytical study of capture time to a horizontal well, *J. Hydrol.*, *217*, 46–54, 1999.

Zhang, D., *Stochastic Methods for Flow in Porous Media: Coping With Uncertainties*, 350 pp., Academic, San Diego, Calif., 2002.

Zhang, D., and Z. Lu, Stochastic analysis of flow in a heterogeneous unsaturated-saturated system, *Water Resour. Res.*, *38*(2), 1018, doi:10.1029/2001WR000515, 2002.

Zhang, D., and S. P. Neuman, Eulerian-Lagrangian analysis of transport conditioned on hydraulic data: 1. Analytical-numerical approach, *Water Resour. Res.*, *31*(1), 39–51, 1995.

Zhang, D., and C. L. Winter, Nonstationary stochastic analysis of steady-state flow through variably saturated, heterogeneous media, *Water Resour. Res.*, *34*, 1091–1100, 1998.

Zlotnik, V., Effects of anisotropy on the capture zone of a partially penetrating well, *Ground Water*, *35*(5), 842–847, 1997.

Zyvoloski, G. A., B. A. Robinson, Z. V. Dash, and L. L. Trease, Summary of the models and methods for the FEHM application—A Finite-element heat- and mass-transfer code, *LA-13307-MS*, Los Alamos Natl. Lab., Los Alamos, N. M., 1997.

Z. Lu and D. Zhang, Hydrology, Geochemistry, and Geology Group (EES-6), MS T003, Los Alamos National Laboratory, Los Alamos, NM 87545, USA. (zhiming@lanl.gov)